European Journal of Medicinal Chemistry 118 (2016) 9–20

Contents lists available at ScienceDirect

European Journal of Medicinal Chemistry

journal homepage: http://www.elsevier.com/locate/ejmech

Research paper

Combretastatin A-4 derived 5-(1-methyl-4-phenyl-imidazol-5-yl) indoles with superior cytotoxic and anti-vascular effects on chemoresistant cancer cells and tumors

Katharina Mahal [a], Bernhard Biersack [a], Sebastian Schruefer [a], Marcus Resch [b], Ralf Ficner [b], Rainer Schobert [a, *], Thomas Mueller [c]

[a] Organic Chemistry Laboratory, University Bayreuth, 95440 Bayreuth, Germany
[b] Department of Molecular Structural Biology, Georg-August-University Göttingen, 37077 Göttingen, Germany
[c] Department of Internal Medicine IV, Oncology/Hematology, Martin-Luther-University Halle-Wittenberg, 06120 Halle-Saale, Germany

ARTICLE INFO

Article history:
Received 18 March 2016
Received in revised form
15 April 2016
Accepted 16 April 2016
Available online 19 April 2016

Keywords:
Imidazole
Indole
Anticancer drugs
Combretastatin A-4
Vascular-disrupting agents
Mouse tumor xenografts

ABSTRACT

5-(1-Methyl-4-phenyl-imidazol-5-yl)indoles **5** were prepared and tested as analogs of the natural vascular-disrupting agent combretastatin A-4 (CA-4). The 3-bromo-4,5-dimethoxyphenyl derivative **5c** was far more active than CA-4 with low nanomolar IC_{50} concentrations against multidrug-resistant KB-V1/Vbl cervix and MCF-7/Topo mamma carcinoma cells, and also against CA-4-resistant HT-29 colon carcinoma cells. While not interfering markedly with the polymerization of tubulin *in vitro*, indole **5c** completely disrupted the microtubule cytoskeleton of cancer cells at low concentrations. It also destroyed real blood vessels, both in the chorioallantoic membrane (CAM) of fertilized chicken eggs and within tumor xenografts in mice, without harming embryo or mouse, respectively. Indole **5c** was less toxic than CA-4 to endothelial cells, fibroblasts, and cardiomyocytes. In highly vascularized xenograft tumors **5c** induced distinct discolorations and histological features typical of vascular-disrupting agents, such as disrupted vessel structures, hemorrhages, and extensive necrosis. In a first preliminary therapy trial, indole **5c** retarded the growth of resistant xenograft tumors in mice.

1. Introduction

The natural tubulin binding agent combretastatin A-4 (CA-4, Fig. 1) was isolated from the bark of the South African Cape Bush-willow (*Combretum caffrum*). Its water soluble phosphate prodrug Zybrestat™ (fosbretabulin) has entered advanced clinical trials that revealed its tumor-selective angiotoxicity, even in multidrug-resistant tumors [1,2]. However, due to its insufficient *in vivo* cytotoxicity it had to be applied in combination with other drugs such as carboplatin, paclitaxel or the anti-angiogenic agent bevacizumab [3,4]. The related combretastatin A-1 and its bisphosphate prodrug OXi4503 also proved efficacious against certain tumor cells in *in vivo* models for which their redox-active catechol moiety was believed to be responsible [5,6]. A drawback of combretastatins is the tendency of their *Z*-alkene to isomerize to a biologically inactive *E*-isomer in protic solvents. So far, the search for chemically more stable derivatives has led to compounds with the alkene adopting a fixed *Z*-configuration, e.g., by being part of a heterocycle [7]. Some 4,5-diaryloxazoles, -imidazoles, and -1,2,3-triazoles of this type actually retained the cytotoxicity and tubulin affinity of the parent combretastatins [8,9]. Among these were orally applicable, water soluble derivatives with advantageous pharmacokinetics and distinct *in vivo* activity such as the imidazole **1** [8]. In another study 3-halo- and 3-aminostilbenes **2**, structurally reminiscent of combretastatin A-3, showed increased affinity for tubulin and a more selective activity profile against tumor cells with potential to overcome drug resistance [10]. Yet, both structure variants have their shortcomings. Derivative **1** is inferior to combretastatin A-4 with respect to cytotoxicity while the analogous oxazoles are hampered with unsatisfactory pharmacological properties [8]. The halo combretastatins **2** prepared by Pettit et al. were quite active yet chemically unstable and required formulations as phosphate prodrugs in order to reach sufficient water solubility and uptake rates [10].

* Corresponding author.
E-mail address: rainer.schobert@uni-bayreuth.de (R. Schobert).

http://dx.doi.org/10.1016/j.ejmech.2016.04.045
0223-5234/

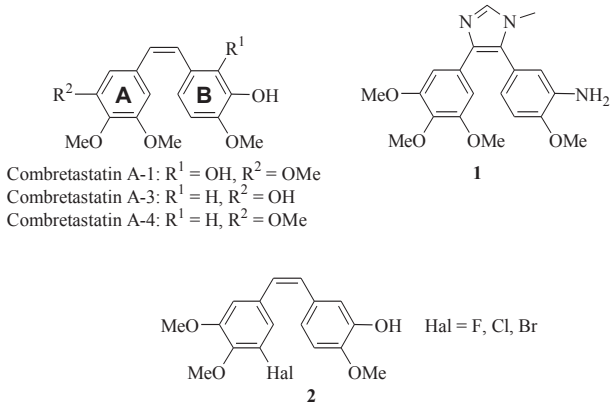

Fig. 1. Combretastatins A-1, A-3, and A-4 and known analogs **1** and **2**: potent inhibitors of tubulin polymerization. Designation of A- and B-ring in the natural drugs combretastatin A.

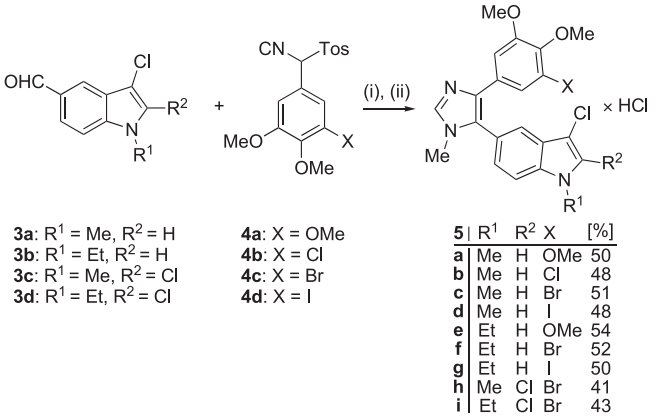

Scheme 1. Reagents and conditions: (i) TosMIC reagent **4**, $MeNH_2$, AcOH, EtOH, reflux, 2 h, then **3**, K_2CO_3, EtOH, reflux, 3 h; (ii) 3 M HCl/dioxane, CH_2Cl_2, r.t., 15 min.

CA-4 fragments were also covalently combined with other tubulin modifier motifs such as indoles. For instance, Dalton et al. disclosed the antitumoral 2-(trimethoxybenzoylphenyl) substituted indole I-387 [11]. Romagnoli et al. reported a 2-aroyl-3-amino derivative which inhibited the growth of breast cancer cells [12]. Simoni et al. prepared an (*N*-methylindol-5-yl)stilbene which caused growth inhibition of triple-negative MDA-MB-231 breast cancer cells [13]. Welsh et al. reported a triazole-bridged indole analog of CA-4 with high tubulin affinity and anticancer activity [14,15]. Pinney et al. developed and optimized 2-aryl-3-aroylindoles such as OXi8006, a highly cytotoxic vascular-disrupting agent [16]. Zhang et al. reported 3-(trimethoxyphenylseleninyl)-1*H*-indoles that bind to tubulin in a similar orientation as CA-4 [17]. Based on the work of Wang et al. our group developed a water-soluble hydrochloride of an *N*-methyl-(3-chloroindol-5-yl)imidazole analog of combretastatin A-4 which was far more cytotoxic against topotecan-resistant (BCRP-positive) MCF-7 breast cancer cells than CA-4 [8,18]. We also prepared CA-4 analogous imidazoles with *meta*-halo-substituted A-rings that had an improved anticancer activity [18,19]. Herein, we continue this work and report on new CA-4 analogous imidazoles with 5-indole residues and their superior anticancer and antivascular properties *in vitro* and *in vivo* when compared with the lead compound CA-4 and with previously published indole **5a** that had been tested only on two cancer cell lines before [8].

2. Results and discussion

2.1. Chemistry

The 5-formylindole derivatives **3a-d** and the TosMIC reagents **4a-d** were prepared according to literature procedures [8,18]. The aldehydes **3a-d** were treated with $MeNH_2$ to give the respective imines, which were reacted with the TosMIC reagents **4a-d** under basic conditions to give the corresponding new *N*-methyl imidazoles **5b-i** (Scheme 1). The known compound **5a** was prepared analogously [8]. All compounds **5** were finally converted with 3 M HCl in dioxane to the corresponding hydrochlorides, which were purified by recrystallization. 5-Formylindoles that lacked a 3-chloro substituent gave no stable hydrochlorides but underwent a rapid degradation with dark red discoloration.

2.2. Biological evaluation

2.2.1. Cytotoxicity

The growth inhibitory activity of the compounds **5a-i** against a panel of cancer cell lines was tested via MTT assays and compared with that of CA-4 (Table 1). Though the lead compound CA-4 displayed the greatest cytotoxicity against highly proliferative 518A2 melanoma cells, it showed only moderate activity against the multidrug-resistant cervix and breast carcinoma cell lines KB-V1/Vbl and MCF-7/Topo. HT-29 colon carcinoma cells were resistant to CA-4 by overexpression of the MRP-1 (multidrug-resistance protein) type ABC (ATP-binding cassette) transporter which detoxifies cells from CA-4 [20]. In contrast, the indoles **5a-5h** were active against the resistant cell lines with nanomolar IC_{50} values. The *N*-methyl indoles **5a-5d** were particularly active at IC_{50} values in the two-digit nanomolar range. Compounds **5a** bearing the original trimethoxy A-ring motif, and **5c** featuring a 3-bromo-4,5-dimethoxyphenyl A-ring, were slightly more active against the resistant cancer cells than the chloro- and iodo-derivatives **5b** and **5d**. Within the triad of *N*-ethyl substituted indoles **5e-5g**, only the trimethoxyphenyl derivative **5e** showed a comparable efficacy. Any further substitution at the indole moiety resulted in an attenuated growth inhibition. We hypothesize that the cell growth inhibiting effect of the compounds **5a-i** might be correlated to their ability to bind to tubulin as reported for CA-4.

The best indole compounds **5a** and **5c** were additionally tested against HCT-116 colon carcinoma cells with either a functional tumor suppressor protein p53 (wildtype, wt) or a knocked-out p53 (HCT-116 *p53*−/−). While the IC_{50} values of CA-4 and **5c** were similar against both cell lines, the trimethoxyphenyl derivative **5a** was more cytotoxic against p53-wildtype cells (Table 2).

To assess the selectivity of the highly active derivatives **5a** and **5c** for cancer over non-malignant cells, we also determined their IC_{50} values against primary fibroblasts (CHF) and cardiomyocytes (CCM) that were explanted from chicken embryos (Table 3). All values for CHF were in the micromolar range with compound **5c** being least cytotoxic. It also affected cardiomyocytes to a lesser extent than CA-4 and derivative **5a**. The distinct *in vitro* cytotoxicity of the anticancer drug doxorubicin against cardiomyocytes is correlated with its severe cardiotoxic side-effects *in vivo* [22]. We therefore conclude that the bromo substituted indole **5c** with the best selectivity profile and the least toxic effects on chicken fibroblasts and cardiomyocytes will probably be the one with the lowest general toxicity in subsequent *in vivo* experiments. It is worth noting that the endothelial cell line included in our growth inhibition tests (Table 1) was less affected by **5a** and **5c** than by CA-4 and that endothelial damage was also reported to be responsible for cardiotoxic side-effects of some tubulin-binding agents [23]. However, Ea.hy926 is a hybrid cell line that does not fully reflect the

Table 1
Inhibitory concentrations IC_{50} [nM] of combretastatin A-4 (CA-4) and the indoles **5a-i** when applied to various human cancer cell lines and Ea.hy926 hybrid endothelial cells.

Cell line		518A2	HT-29	KB-V1/Vbl	MCF-7/Topo	Ea.hy926
CA-4	[b]	1.8 ± 0.1 [c]	>5000	300 ± 200 [c]	154 ± 33 [c]	11.0 ± 2.0 [c]
5a	[a]	65.4 ± 7.3	26.2 ± 5.2	26.0 ± 2.9	20.2 ± 1.2	24.6 ± 2.8
	[b]	18.2 ± 0.5	15.6 ± 2.4			
5b	[a]	174 ± 13.7	33.7 ± 1.7	37.9 ± 2.1	26.9 ± 7.2	*n. d.*
	[b]	32.4 ± 2.0	31.4 ± 5.8			
5c	[a]	51.9 ± 6.3	31.3 ± 4.7	25.4 ± 2.8	18.8 ± 1.4	29.9 ± 4.5
	[b]	28.2 ± 1.3	23.4 ± 5.9			
5d	[a]	56.7 ± 4.8	35.1 ± 1.2	49.8 ± 7.6	53.3 ± 2.3	*n. d.*
	[b]	35.7 ± 2.9	39.7 ± 4.8			
5e	[a]	739 ± 121	75.8 ± 8.9	33.2 ± 10	30.2 ± 1.7	
	[b]	33.0 ± 8.0	43.4 ± 7.7			
5f	[a]	216 ± 76	246 ± 37	48.4 ± 1.7	91.3 ± 9.9	
	[b]	82 ± 4.1	116 ± 22			
5g	[a]	211 ± 51	482 ± 34	83.2 ± 8.5	81.2 ± 10.1	
	[b]	168 ± 30	178 ± 37			
5h	[a]	292 ± 43	903 ± 100	456 ± 11	208 ± 38	
	[b]	223 ± 44	223 ± 44			
5i	[a]	>1000	>1000	>1000	489 ± 39	
	[b]	767 ± 88	793 ± 89			

Values are derived from dose–response curves obtained by measuring the percentage of viable cells relative to untreated controls after 24 h [a] or 72 h [b] exposure to the test compounds using an MTT assay; human cancer cell lines: 518A2 melanoma, HT-29 colon, KB-V1/Vbl cervix, MCF-7/Topo breast carcinoma. Ea.hy926: endothelial hybrid cells. [c] Values from earlier publications [18,21]. Values represent means of four independent experiments. Conspicuous values are highlighted in gray.

Table 2
Inhibitory concentrations IC_{50} [nM, 72 h][a] of combretastatin A-4 (CA-4) and the indoles **5a** and **5c** for the growth of human p53-wildtype and p53-negative HCT-116 colon carcinoma cells.

Cell line	CA-4	**5a**	**5c**
HCT-116 wt	2.6 ± 0.2	9.5 ± 1.5	27.4 ± 1.5
HCT-116 *p53−/−*	3.4 ± 0.4	26.2 ± 3.0	21.3 ± 2.3

[a] Values are derived from dose–response curves obtained by measuring the percentage of viable cells relative to untreated controls after 72 h. Values represent means of three independent experiments.

Table 3
Inhibitory concentrations IC_{50} [μM, 48 h][a] of CA-4 and the indoles **5a** and **5c** on the growth of primary chicken fibroblasts (CHF) and chicken cardiomyocytes (CCM) and relative cancer cell selectivity (selectivity index).

Cell line	CA-4	**5a**	**5c**
CHF	5.48 ± 0.24	11.61 ± 1.5	23.02 ± 1.8
CCM	0.874 ± 0.08	1.87 ± 0.4	3.97 ± 1.3
selectivity index	1.81	2.99	3.19

[a] Values are derived from dose–response curves obtained by measuring the percentage of viable cells relative to untreated controls after 48 h. Values represent means of three independent experiments.

sensitivity of primary endothelial cells.

2.2.2. Cell cycle interference

The observed growth inhibition by the best two indoles **5a** and **5c** might be due to induction of apoptosis or inhibition of the cell cycle progression as reported for many tubulin binding agents [24]. In cell cycle analyses with 518A2, HCT-116 and MCF-7/Topo cells after 24 h incubation with the test compounds, we found an increase in apoptotic cells, but also a significant accumulation of treated cells in the G2/M phase (Table S1, Supplementary data). The cell cycle progression of HT-29 colon carcinoma cells was arrested by **5c** mainly in mitosis as observed via concomitant immunostaining of phosphorylated histone H3 (phospho-H3) as a mitosis marker (Table 4; Fig. S1, Supplementary data).

2.2.3. Tubulin affinity

To check the hypothesis that the compounds' cytotoxicity correlates with their affinity for tubulin, we performed polymerization assays with purified porcine tubulin (Fig. 2a). CA-4 was used as a control with known high tubulin affinity. 5 μM of CA-4 and indole **5a** were sufficient to impair the polymerization of tubulin heterodimers to microtubules, though **5a** was less active at equimolar concentrations. 5 μM of indole **5c** slowed down the rate of the polymerization, but could not suppress it. This divergent tubulin affinity of compounds **5a** and **5c** is somewhat surprising, given their comparable IC_{50} values in the cytotoxicity tests with HT-29, KB-V1/Vbl and MCF-7/Topo cancer cells. The assumption of an additional mode of cytotoxic action of either **5a** or **5c** would also be supported by their distinctly different activities against the HCT-116 (wt) carcinoma cells (Table 2).

By molecular docking studies we found that **5c** can adopt a favourable binding mode within the tubulin heterodimer (with a theoretical $E_{bind} = -8.8$ kcal/mol; Fig. 2b left) that differs from that of the lead compound CA-4, and a slightly less favourable binding mode (with a theoretical $E_{bind} = -8.3$ kcal/mol; Fig. 2b right) similar to that of CA-4.

Like CA-4, indole **5c** can bind to the colchicine binding pocket within the beta-tubulin subunit of the tubulin heterodimer, yet in a different orientation (Fig. 2b, left). In this conformation, the indole moiety is placed in the hydrophobic pocket made up by Leu-β248, Ala-β250, Ala-β316, Val-β318, Ala-β354, Ile-β378, where the A-ring of colchicine and CA-4 is bound [25]. The *p*-methoxy group of the phenyl ring (corresponding to the A-ring of CA-4) is locked by Vander-Waals interactions with a methylene group of Lys-β254 and the *m*-methoxy oxygen is engaged in a hydrogen bond with the side-chain amine of Asn-α101. In addition, the non-methylated

Table 4
Percentage of HT-29 colon carcinoma cells in cell cycle phases after treatment with DMSO (control), combretastatin A-4 (5 μM) or indole **5c** (50 and 100 nM) for 24 h.

Cell cycle phase (%)	Control	CA-4	100 nM **5c**	50 nM **5c**
G1	68.1 ± 0.3	51.4 ± 0.8	12.0 ± 0.3	43.5 ± 2.8
S	13.7 ± 0.3	18.6 ± 1.8	8.0 ± 2.9	13.5 ± 0.4
G2	15.6 ± 0.1	18.2 ± 1.0	4.6 ± 0.2	15.2 ± 3.2
mitosis	3.2 ± 0.1	10.2 ± 0.4	77.8 ± 3.8	28.0 ± 1.1

Values derived from flow cytometric cell cycle analyses with HT-29 cells double-stained for their DNA content with propidium iodide and a phospho-histone H3 mitosis marker.

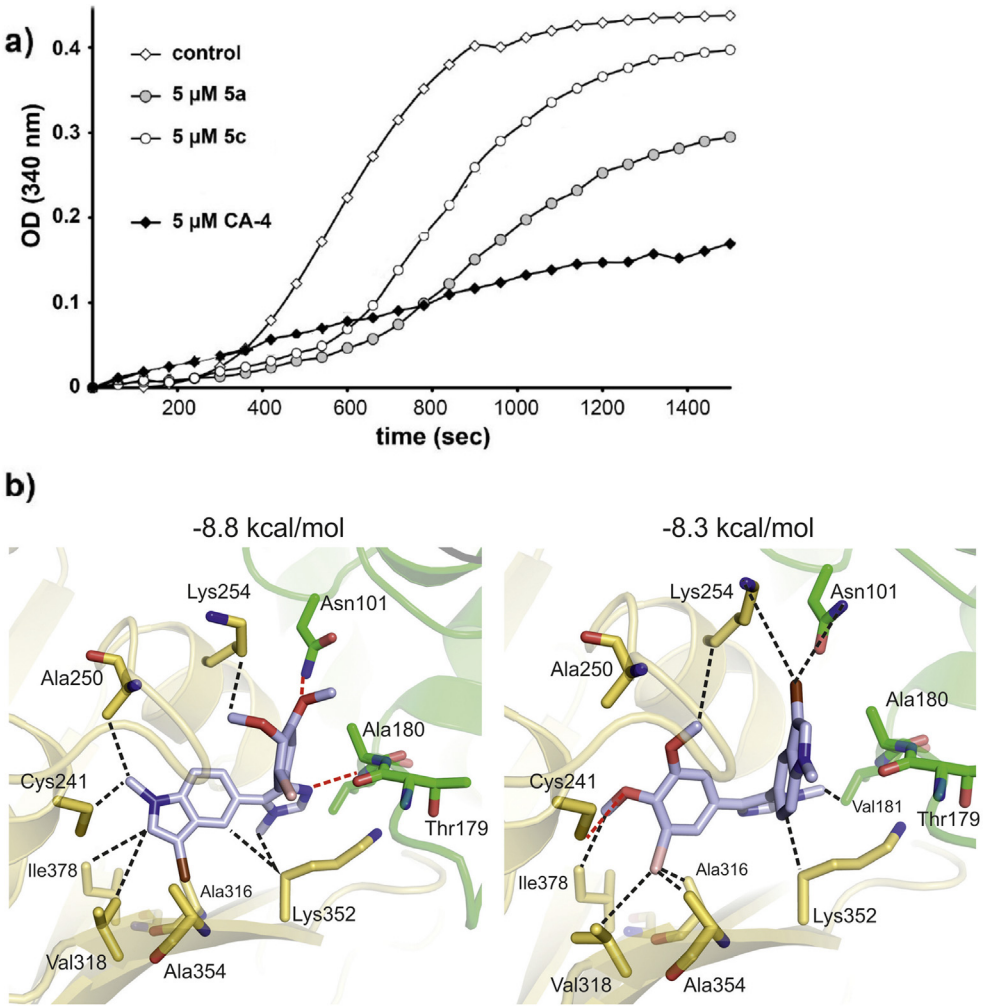

Fig. 2. Interference of indoles **5a** and **5c** with the polymerization of tubulin. **a**) Tubulin polymerization curves in the absence (control) or presence of combretastatin A-4 (CA-4), or **5a**, or **5c** recorded by the optical density (OD) at 340 nm wavelength. **b**) Docking studies: *left*: proposed binding mode of **5c** (carbon colored light blue) in the binding pocket within the beta-tubulin subunit of a bovine tubulin (pdb-code 1SA0). The energetically more favourable orientation with a theoretical $E_{bind} = -8.8$ kcal/mol differs from that of CA-4. The indole moiety is placed in the hydrophobic cleft made up by the side-chains of Leu-248, Ala-250, Ala-316, Val-318, Ala-354, and Ile-378, with carbon colored light yellow (β chain), sulfur yellow, nitrogen blue, oxygen red. *Right*: proposed binding mode of **5c** (carbon colored light blue) in the binding pocket within the beta-tubulin subunit. The energetically slightly less favourable orientation with a theoretical $E_{bind} = -8.3$ kcal/mol resembles that known of CA-4, with the phenyl moiety placed in the hydrophobic cleft made up by the side-chains of Leu-248, Ala-250, Ala-316, Val-318, Ala-354, and Ile-378. (For interpretation of the references to color in this figure legend, the reader is referred to the web version of this article.)

nitrogen of the imidazole ring is able to form a hydrogen bond with the backbone amide hydrogen of Val-α181 whereas the N-methyl group of the imidazole ring favorably interacts with the methylene of Lys-β352. The calculated tubulin binding energy of **5c** ($E_{bind} = -8.8$ kcal/mol) is comparable with that of colchicine ($E_{bind} = -9.0$ kcal/mol).

In the second, energetically slightly less favourable orientation (Fig. 2b, right), the phenyl ring of **5c** is placed in the hydrophobic pocket, like the A-rings of colchicine and CA-4 [25]. The *p*-methoxy group of the phenyl ring can link up to Ile-β378 by Van-der-Waals interactions, while the *p*-methoxy oxygen is engaged in a hydrogen bond with the sulfhydryl side-chain of Cys-β241. The *m*-methoxy group of the phenyl ring can interact with a methylene group of Lys-β254. The bromo substituent is placed in the hydrophobic pocket made up by Ala-β316, Val-β318, Ala-β354, Ile-β378. The chloro residue of the indole is oriented towards the amino side-chain of Lys-β254 and the side-chain amine of Asn-α101. The N-methyl group of the imidazole can connect via Van-der-Waals interactions to the Val-β181 side-chain. In addition, the indole ring favorably interacts with the methylene of Lys-β352.

The existence of two energetically close binding orientations of **5c** might even go some way towards explaining its weak interference with tubulin *in vitro* and its reduced toxicity to non-malignant cells by assuming a metastable conformation of tubulin ligated with **5c** with retarded polymerization dynamics.

Immunofluorescence microscopic analyses of the microtubule-disrupting effects of **5a** and **5c** in 518A2 melanoma cells revealed a similar efficacy of both derivatives (Fig. 3). Incubation with 100 nM of **5c** for 24 h led to an extensive destruction of the microtubular network while residual microtubular structures remained after incubation with **5a**. These differences in the effects of **5a** and **5c** on cellular microtubules mirror their different IC_{50} (24 h) values against this cell line in the MTT tests (Table 1) and might be due to different uptake rates.

2.2.4. *Antivascular effects*

Since microtubule disruption is a major aspect of the anti-vascular activity of CA-4 and its prodrug CA-4-phosphate [26,27],

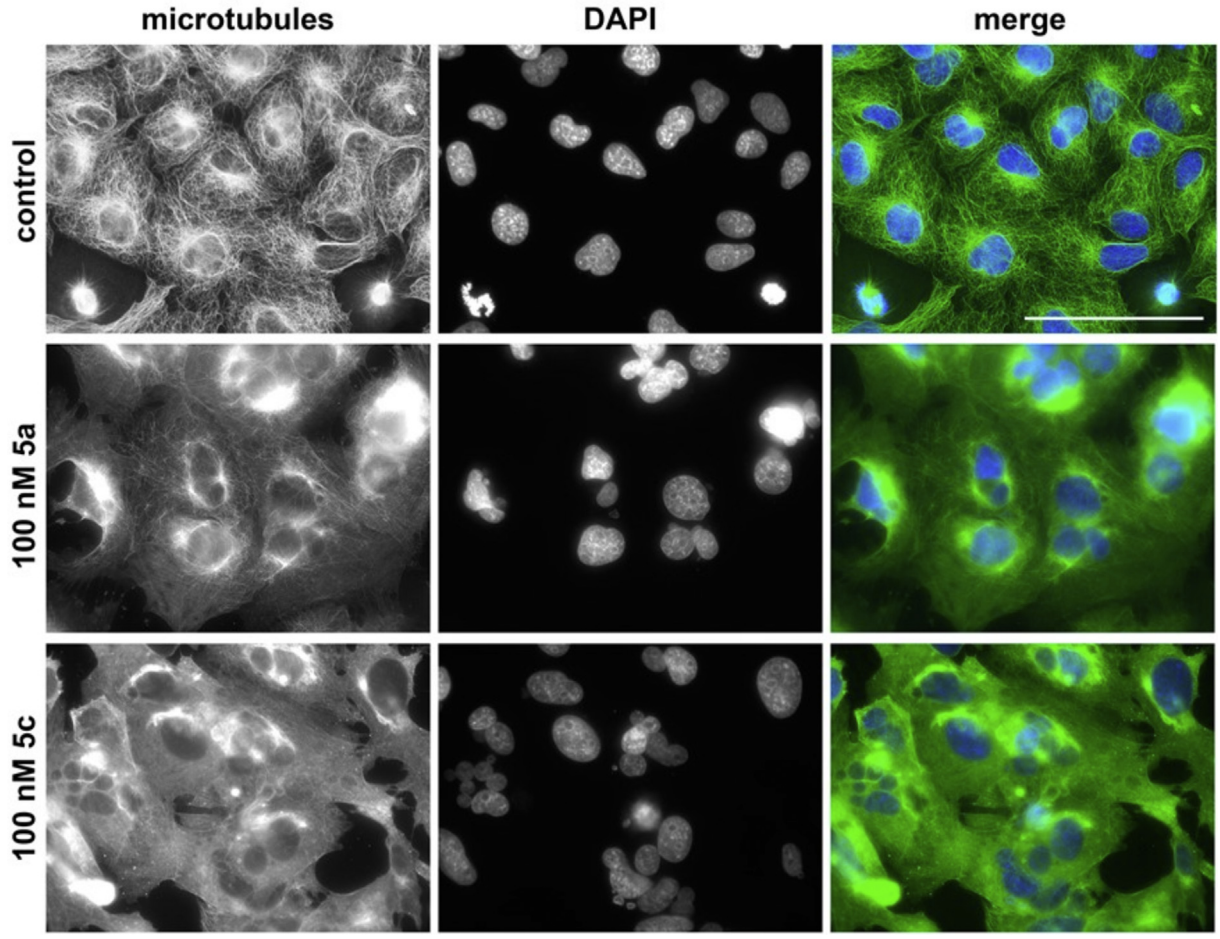

Fig. 3. Fluorescence microscopic visualization of microtubules (anti-alpha-tubulin) and nuclei (DAPI) in 518A2 melanoma cells after 24 h incubation with DMSO (control) or 100 nM of **5a** or **5c**. 400-fold magnification, scale bar: 100 μm.

we performed *in vitro* tube formation assays with Ea.hy926 endothelial cells to qualitatively assess any vascular-disrupting effects of the best performing indoles **5a** and **5c**. When applied at 250 nM concentrations, both indoles disrupted preformed vessel-like tubular networks of these cells to an extent comparable with the effect of 100 nM CA-4 (Fig. 4). The compounds induced a retraction of cells to the nodes, a change of their morphology from stretched to rounded, and a loss of the cell–cell connections that build up the blood vessel-like mesh network.

This effect was also investigated *in vivo* by using the chorioallantoic membrane (CAM) of fertilized chicken eggs as a model system for rapidly developing blood vessels (Fig. 5).

Interestingly, 5 nmol of the trimethoxy derivative **5a** were strongly toxic to the chicken embryos. After 12 h incubation, existing blood vessels had been almost completely disrupted and a pronounced hemorrhage was observed on the CAM suggesting that chicken embryos also suffered from internal hemorrhage. The bromo derivative **5c** was much better tolerated while retaining a strong vascular-disrupting effect even when only 2.5 nmol were applied. The lethality of chicken embryos was significantly reduced (Table S2, Supplementary data). Though existing blood vessels were destroyed and hemorrhage of blood vessel outgrowths on the CAM could be observed, the blood vessel system was able to regenerate within the following 24–48 h and embryos apparently developed normally (data not shown).

We also tested indole **5c** on microtumor-xenografts of HT-29 colon carcinoma cell pellets in matrigel grafted on the CAM of fertilized chicken eggs (Fig. 6). Within a couple of days these microtumors grew into the CAM and recruited new blood vessels in their vicinity, either by secreting growth factors or via inflammation as a consequence of grafting. They can also interact with the chicken CAM tissue in a way reminiscent of mouse xenograft models [28]. 24 h after treatment with **5c** a partial destruction of surrounding blood vessels and a faint hemorrhage within the HT-29 microtumor was observed. HE-staining of untreated CAM-tumor cross sections (Fig. 6, right column) revealed some blood vessels surrounded by HT-29 tumor cells at the interface between the tumor pellet and the CAM or even blood vessels that had already grown into the developing tumor graft. Intact blood vessels were not found in CAM-tumor cross sections treated with **5c**, and a great number of erythrocytes corroborated the macroscopically observed hemorrhage. In addition, a retraction of individual tumor cells within the pellet and a loss of cell–cell interactions as a consequence of severe cytoskeletal damage or even induction of apoptosis was observed. This remarkable vascular-disrupting activity occurs at drug concentrations not compromising the embryo's vitality.

2.2.5. Animal studies

We also investigated the vascular-disrupting activity of **5c** in highly vascularized xenograft tumors of the 1411HP germ cell tumor cell line in mice which is an established animal model, previously used for testing other vascular-disrupting agents [18,21]. As a second model we used the ovarian carcinoma cell line A2780cis

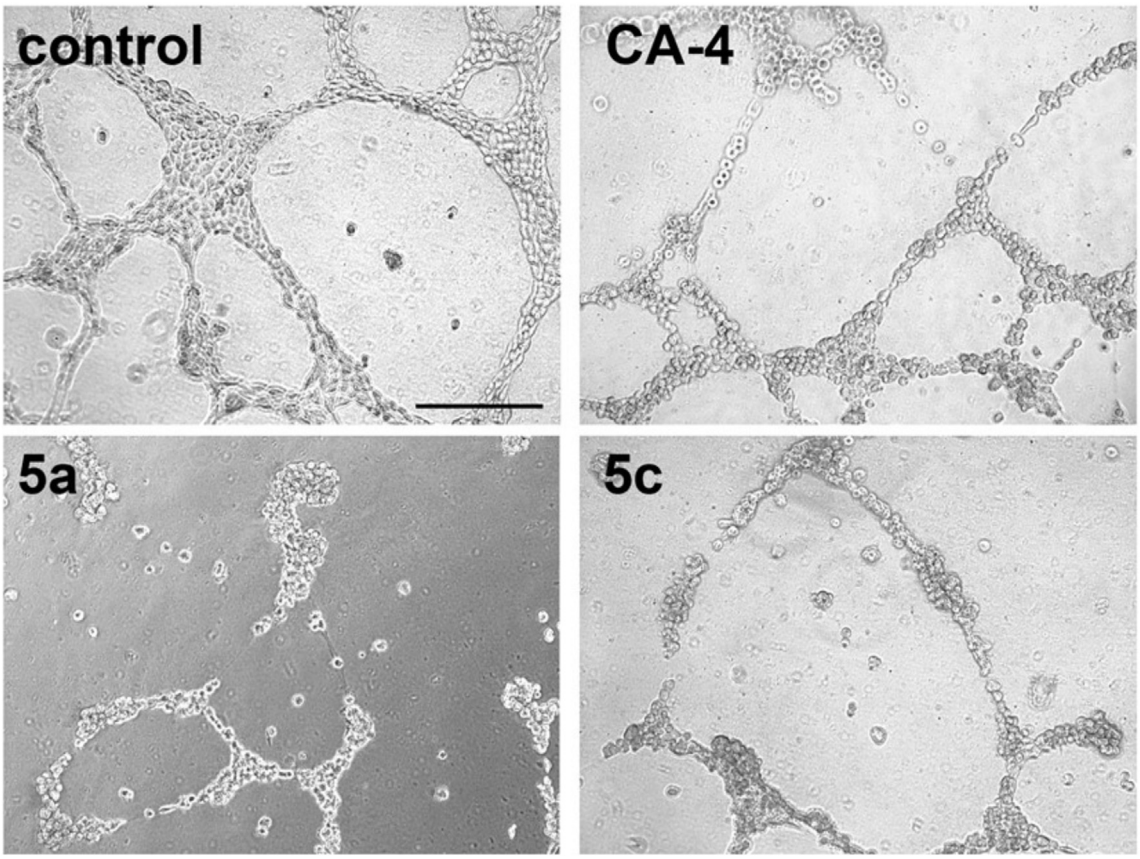

Fig. 4. Effects of CA-4 and of the indoles **5a** and **5c** on the propensity of Ea.hy926 endothelial cells to form blood vessel-like networks when grown on matrigel layers. Cells grown for 12 h and incubated with CA-4 (100 nM), **5a** or **5c** (250 nM) for additional 16 h were documented by light microscopy (100-fold magnification, scale bar: 200 μm).

which also readily forms highly vascularized xenograft tumors. Both cell lines are resistant to various anticancer drugs. A single treatment of the xenograft bearing mice with 100 mg/kg body weight of **5c** induced a distinct discoloration in both tumor types within 24 h due to intratumoral hemorrhage (Fig. 7A). Histological examination of tumors of treated mice revealed typical features of vascular-disrupting agents, such as disrupted vessel structures, hemorrhage and extensive necrosis (Fig. 7B–E).

To prove the anticancer efficacy of **5c** in resistant tumors we finally undertook preliminary therapy trials in mice bearing A2780cis tumors. Treatment with **5c** resulted in a distinct tumor growth retardation relative to controls (Fig. 8). Although this has to be confirmed in a larger trial these findings recommend **5c** as a promising drug candidate for the treatment of resistant tumors.

3. Conclusions

The new imidazolylindoles **5** are conjugates of two pharmacophores of vascular-disrupting agents, borrowed from the natural combretastatins A and from known synthetic indoles. The intention was to overcome the shortcomings of CA-4, such as insufficient cytotoxicity, cancer selectivity, stability, and tolerance. We could indeed identify some derivatives of general structure **5** that lived up to this objective. All derivatives **5a-d** featuring an N-methyl substituted indole and a halo-dimethoxy or trimethoxy substituted A-ring were highly active against all tested tumor cell lines, including multidrug-resistant and CA-4-resistant ones. This is in keeping with tubulin docking studies which pinpointed crucial binding interactions originating from these residues. There are subtle differences in the modes of action of CA-4 and active compounds **5**. The latter gave rise to a stronger mitotic arrest in cancer cells and a more pronounced disruption of their microtubular cytoskeleton, although they did not interfere with purified tublin *in vitro* as much as CA-4. The vascular-disrupting effects of the most active compound **5c** *in vitro* and *in vivo* were comparable to or better than those of the lead compound CA-4. It also showed a better tolerance in non-malignant cells and animals and a distinct tumor growth inhibiting effect in preliminary animal studies. The fact that minute alterations of substituents at the periphery of the indole ring, e.g., when going from R^2 = H in **5c** to R^2 = Cl in **5h**, made such a big difference in activity, leaves ample room for further drug optimisation.

4. Experimental section

4.1. Chemistry

4.1.1. General

IR spectra: FT-IR spectrophotometer equipped with an ATR unit. ^{1}H NMR and ^{13}C NMR spectra: Bruker DRX 500 and DRX 300 spectrometer; chemical shifts are given in parts per million using the residual solvent peak as an internal standard; coupling constants (*J*) are quoted in Hz. Mass spectra: Thermo Finnigan MAT 8500 spectrometer under EI (70 eV) conditions using a MAT SS 300 data system. Microanalyses indicated by the symbols of the elements were within ±0.4% of the theoretical values.

4.1.2. 3-Chloro-1-methyl-5-[1-methyl-4-(3-chloro-4,5-dimethoxyphenyl)-imidazol-5-yl]indole hydrochloride (**5b**)

N-Methyl-3-chloroindole-5-carboxaldehyde **3a** (81 mg,

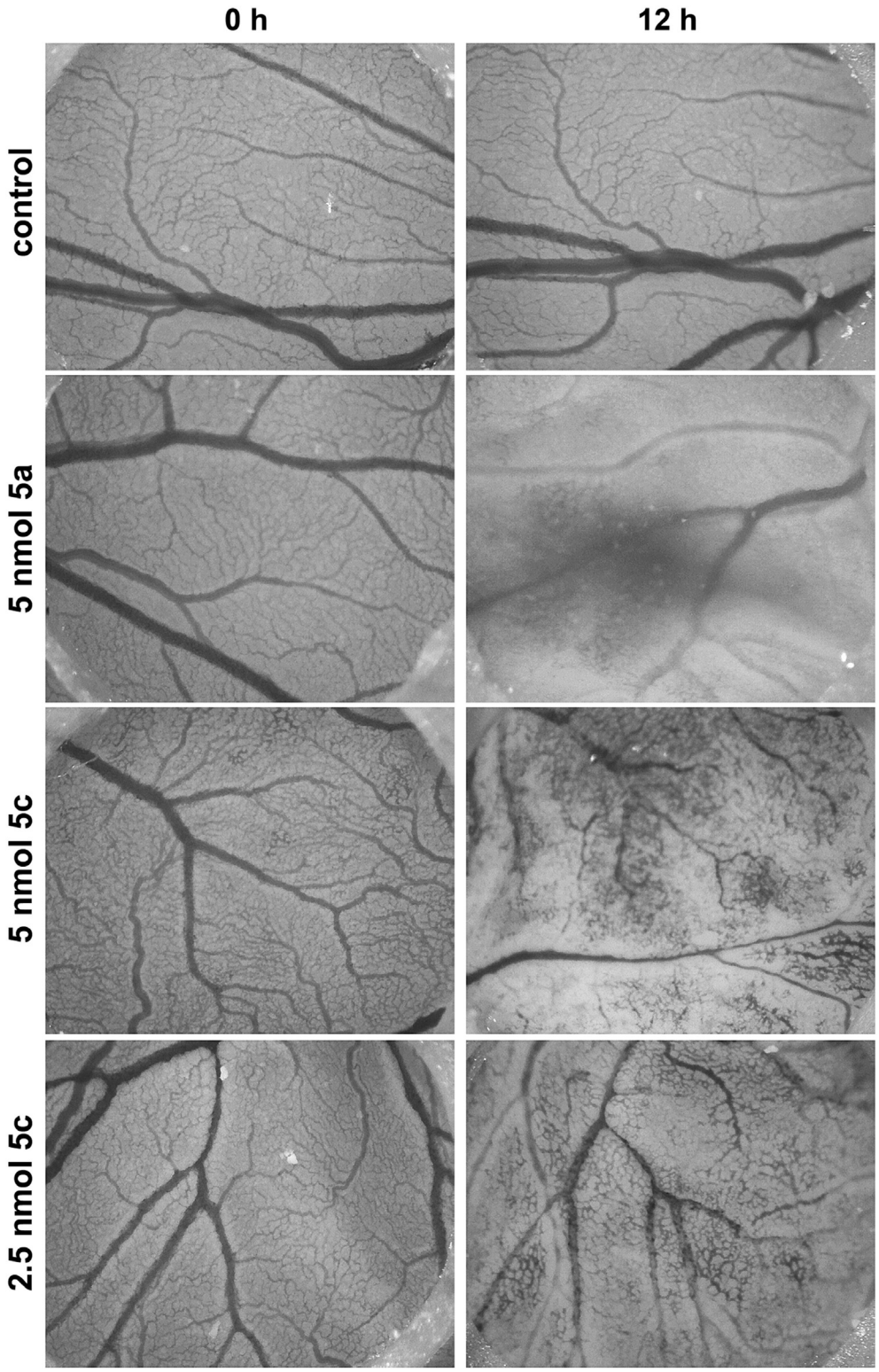

Fig. 5. Effects of the indoles **5a** and **5c** on developing blood vessels in the chorioallantoic membrane (CAM) of fertilized chicken eggs (6 d after fertilization). Dilutions of the compounds (2.5 nmol or 5 nmol in PBS) were directly applied within rings of silicon foil (6 mm diameter) and alterations 12 h post application were documented with a stereomicroscope (60-fold magnification).

0.42 mmol), 33% $MeNH_2$/ethanol (260 μL, 2.10 mmol) and acetic acid (150 μL) were refluxed in ethanol (15 mL) for 2 h, then TosMIC reagent **4b** (153 mg, 0.42 mmol) and K_2CO_3 (500 mg, 3.62 mmol) were added and the reaction mixture was stirred under reflux for 3 h. The solvent was evaporated, the residue was suspended in water and extracted with ethyl acetate. The organic phase was dried over Na_2SO_4, concentrated in vacuum and purified by column chromatography to give the free base of **5b** (colorless oil; $R_f = 0.62$,

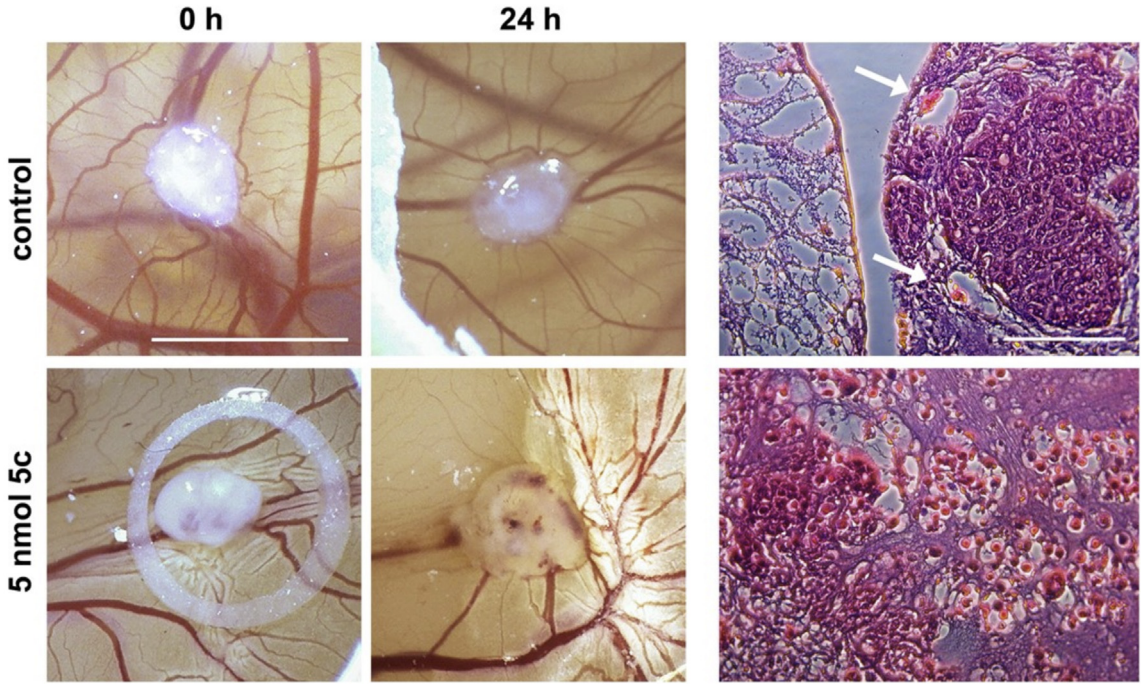

Fig. 6. Effects of indole **5c** on developing blood vessels and HT-29 micro-xenografts 24 h post application on the chorioallantoic membrane (CAM) of fertilized chicken eggs. HT-29 tumor pellets grafted on the CAM for 48 h and then treated with the control DMSO (*top row*) or 5 nmol of **5c** in PBS (application outside the silicon ring; *bottom row*) for 24 h, documentation by stereomicroscopy (10-fold magnification, scale bar: 6 mm). *Right column*: HE-staining of HT-29 micro-xenograft cross sections, arrows indicate intact blood vessels surrounded by HT-29 cells, documentation by light microscopy (320-fold magnification, scale bar: 100 μm). (For interpretation of the references to color in this figure legend, the reader is referred to the web version of this article.)

ethyl acetate/methanol 95:5). The free base was dissolved in CH_2Cl_2 (5 mL) and treated with 3 M HCl/dioxane (1 mL). After stirring for 10 min the solvent was evaporated and the residue was recrystallized from CH_2Cl_2/*n*-hexane. Yield: 98 mg (0.20 mmol, 48%); colorless solid; mp 198 °C; UV (MeOH) λ_{max} (ε) 230 (30,800); ν_{max} (ATR)/cm^{-1}: 3392, 2941, 2845, 2602, 1622, 1565, 1542, 1493, 1464, 1456, 1318, 1239, 1115, 1046, 996, 971, 871, 852, 803; ^{1}H NMR (300 MHz, DMSO-d_6): δ 3.61 (6 H, s), 3.72 (3 H, s), 3.86 (3 H, s), 6.99 (1 H, d, ^4J 2.1 Hz), 7.20 (1 H, d, ^4J 2.1 Hz), 7.34 (1 H, dd, ^3J 9.4 Hz, ^4J 1.6 Hz), 7.7–7.8 (3 H, m), 9.32 (1 H, s); ^{13}C NMR (75.5 MHz, DMSO-d_6): δ 33.0, 33.9, 56.0, 60.3, 102.7, 110.8, 111.8, 117.0, 119.5, 120.4, 124.1, 124.5, 125.1, 127.2, 127.9, 128.3, 130.9, 135.6, 136.0, 144.8, 153.4; *m*/*z* (EI) 417 (100) [M$^+$], 415 (68) [M$^+$], 402 (66), 400 (96). Anal $C_{21}H_{19}Cl_2N_3O_2$ (free base; C, H, N).

4.1.3. 3-Chloro-1-methyl-5-[1-methyl-4-(3-bromo-4,5-dimethoxyphenyl)-imidazol-5-yl]indole hydrochloride (*5c*)

Analogously to the synthesis of **5b**, compound **5c** (115 mg, 51%) was obtained from **3a** (81 mg, 0.42 mmol), 33% $MeNH_2$/ethanol (260 μL, 2.10 mmol), acetic acid (150 μL), and **4c** (170 mg, 0.42 mmol); colorless solid of mp 146 °C (ethanol/*n*-hexane); UV (MeOH) λ_{max} (ε) 230 (34,040); ν_{max} (ATR)/cm^{-1}: 3392, 2941, 2591, 1622, 1592, 1544, 1490, 1464, 1406, 1317, 1263, 1239, 1146, 1115, 1042, 995, 973, 874, 853, 809; ^{1}H NMR (300 MHz, DMSO-d_6): δ 3.61 (6 H, s), 3.70 (3 H, s), 3.86 (3 H, s), 7.14 (1 H, d, ^4J 2.1 Hz), 7.26 (1 H, d, ^4J 2.1 Hz), 7.34 (1 H, dd, ^3J 8.5 Hz, ^4J 1.6 Hz), 7.7–7.8 (3 H, m), 9.36 (1 H, s); ^{13}C NMR (75.5 MHz, DMSO-d_6): δ 33.0, 33.9, 56.0, 60.2, 102.7, 111.4, 111.8, 116.9, 117.0, 120.4, 122.3, 124.5, 124.7, 125.1, 127.7, 128.3, 130.9, 135.5, 136.0, 145.9, 153.2; *m*/*z* (EI) 461 (100) [M$^+$], 459 (82) [M$^+$], 446 (59), 444 (57); Anal $C_{21}H_{19}BrCl_2N_3O_2$ (free base; C, H, N).

4.1.4. 3-Chloro-1-methyl-5-[1-methyl-4-(3-iodo-4,5-dimethoxyphenyl)-imidazol-5-yl]indole hydrochloride (*5d*)

Analogously to the synthesis of **5b**, compound **5d** (110 mg, 48%) was obtained from **3a** (81 mg, 0.42 mmol), 33% $MeNH_2$/ethanol (260 μL, 2.10 mmol), acetic acid (150 μL), and **4d** (192 mg, 0.42 mmol); colorless solid of mp 160–165 °C (ethanol/*n*-hexane); ν_{max} (ATR)/cm^{-1}: 3019, 2932, 2572, 1623, 1589, 1544, 1486, 1464, 1406, 1360, 1314, 1260, 1242, 1146, 1115, 1039, 995, 973, 872, 854, 807, 796, 751, 726, 670; ^{1}H NMR (300 MHz, DMSO-d_6): δ 3.57 (3 H, s), 3.62 (3 H, s), 3.67 (3 H, s), 3.87 (3 H, s), 7.20 (1 H, d, ^4J 2.0 Hz), 7.3–7.4 (2 H, m), 7.7–7.8 (3 H, m), 9.34 (1 H, s); ^{13}C NMR (75.5 MHz, DMSO-d_6): δ 33.0, 33.9, 55.8, 59.9, 93.0, 102.7, 111.7, 112.1, 117.0, 120.4, 124.5, 125.1, 125.4, 127.6, 128.1, 128.2, 130.8, 135.5, 136.0, 148.5, 152.0; *m*/*z* (EI) 509 (33) [M$^+$], 507 (100) [M$^+$], 492 (41); Anal $C_{21}H_{19}ClIN_3O_2$ (free base; C, H, N).

4.1.5. 3-Chloro-1-ethyl-5-[1-methyl-4-(3,4,5-trimethoxyphenyl)-imidazol-5-yl]indole hydrochloride (*5e*)

Analogously to the synthesis of **5b**, compound **5e** (104 mg, 54%) was obtained from **3b** (88 mg, 0.42 mmol), 33% $MeNH_2$/ethanol (260 μL, 2.10 mmol), acetic acid (150 μL), and **4a** (150 mg, 0.42 mmol); colorless solid of mp 245 °C (ethanol/*n*-hexane); ν_{max} (ATR)/cm^{-1}: 3984, 2948, 2530, 1617, 1597, 1553, 1519, 1494, 1462, 1445, 1417, 1405, 1337, 1321, 1286, 1261, 1220, 1196, 1161, 1120, 1030, 991, 875, 852, 828, 812, 798, 771, 747, 713; ^{1}H NMR (300 MHz, DMSO-d_6): δ 1.36 (3 H, t, ^3J 7.1 Hz), 3.47 (6 H, s), 3.61 (3 H, s), 3.65 (3 H, s), 4.28 (2 H, q, ^3J 7.1 Hz), 6.81 (2 H, s), 7.35 (1 H, dd, ^3J 8.5 Hz, ^4J 1.6 Hz), 7.73 (1 H, s), 7.8–7.9 (2 H, m), 9.41 (1 H, s); ^{13}C NMR (75.5 MHz, DMSO-d_6): δ 15.4, 33.9, 40.9, 55.6, 60.0, 102.9, 104.4, 111.7, 117.3, 120.7, 122.4, 124.6, 125.3, 126.7, 129.0, 130.3, 135.0, 137.7, 152.8; *m*/*z* (EI) 427 (35) [M$^+$], 425 (100) [M$^+$], 412 (28), 410 (92); Anal $C_{23}H_{24}ClN_3O_3$ (free base; C, H, N).

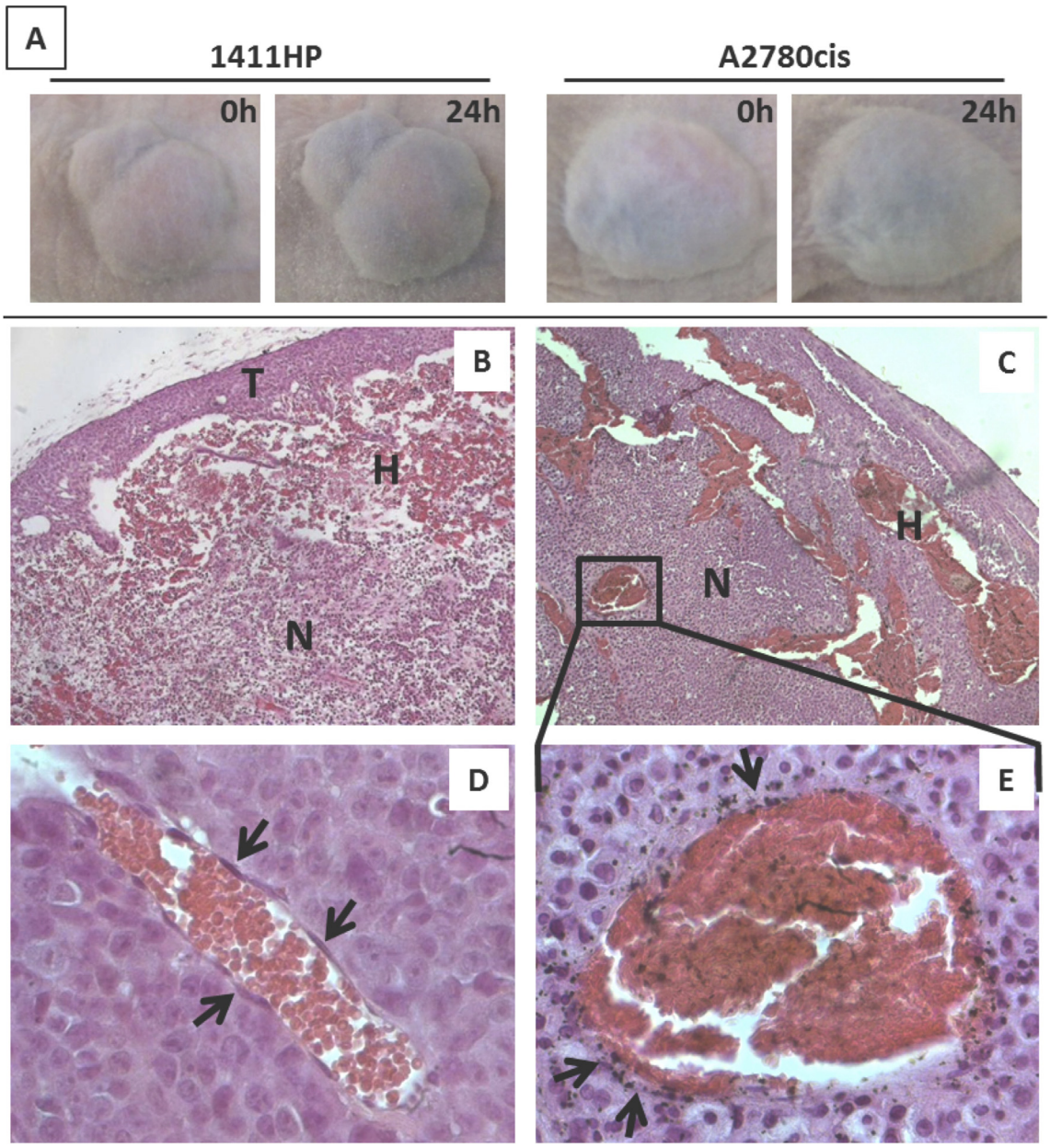

Fig. 7. Vascular-disrupting effects of indole **5c** in nude mouse xenograft tumors. **A**: Discoloration of 1411HP and A2780cis xenograft tumors due to intratumoral hemorrhages 24 h after treatment. **B**: Lateral section of the treated 1411HP tumor shown in A after HE staining featuring hemorrhages (H) and a large necrotic core area (N) surrounded by a cortical layer of vital tumor cells (T). **C**: Lateral section of the treated A2780cis tumor shown in A after HE staining featuring hemorrhages (H) and a core area characterized by early signs of massive necrotic cell death. **D**: Normal blood vessel structure of an untreated A2780cis tumor showing erythrocytes surrounded by an intact endothelial cell layer (black arrows). **E**: Magnified disrupted blood vessel, framed in C, showing agglutinated erythrocytes surrounded by residual cell fragments of the disrupted endothelial cell layer (black arrows) and dying tumor cells. (**B** and **C**: 100-fold magnification, **D** and **E**: 400-fold magnification, zoomed).

*4.1.6. 3-Chloro-1-ethyl-5-[1-methyl-4-(3-bromo-4,5-dimethoxyphenyl)-imidazol-5-yl]indole hydrochloride (**5f**)*

Analogously to the synthesis of **5b**, compound **5f** (110 mg, 52%) was obtained from **3b** (88 mg, 0.42 mmol), 33% $MeNH_2$/ethanol (260 μL, 2.10 mmol), acetic acid (150 μL), and **4c** (172 mg, 0.42 mmol); colorless solid of mp 240 °C (ethanol/*n*-hexane); ν_{max} (ATR)/cm^{-1}: 2946, 2936, 2607, 1623, 1595, 1546, 1490, 1464, 1448, 1407, 1347, 1316, 1262, 1219, 1146, 1115, 1042, 995, 874, 853, 795, 753, 726, 676; ^{1}H NMR (300 MHz, DMSO-d_6): δ 1.37 (3 H, t, ^3J 7.2 Hz), 3.59 (3 H, s), 3.63 (3 H, s), 3.69 (3 H, s), 4.29 (2 H, q, ^3J 7.2 Hz), 7.16 (1 H, d, ^4J 2.1 Hz), 7.25 (1 H, d, ^4J 2.1 Hz), 7.33 (1 H, dd, ^3J 8.5 Hz, ^4J 1.6 Hz), 7.71 (1 H, s), 7.8–7.9 (2 H, m), 9.41 (1 H, s); ^{13}C NMR (75.5 MHz, DMSO-d_6): δ 15.4, 33.9, 40.9, 56.0, 60.2, 103.0, 111.4, 111.8, 116.8, 117.0, 120.5, 122.3, 124.5, 124.6, 125.3, 126.8, 127.6, 130.9, 135.1, 135.4, 145.8, 153.2; *m/z* (EI) 475 (100) [M^+], 473 (77) [M^+], 460 (54), 458 (45); Anal $C_{22}H_{21}BrClN_3O_2$ (free base; C, H, N).

*4.1.7. 3-Chloro-1-ethyl-5-[1-methyl-4-(3-iodo-4,5-dimethoxyphenyl)-imidazol-5-yl]indole hydrochloride (**5g**)*

Analogously to the synthesis of **5b**, compound **5g** (114 mg, 50%) was obtained from **3b** (88 mg, 0.42 mmol), 33% $MeNH_2$/ethanol (260 μL, 2.10 mmol), acetic acid (150 μL), and **4d** (192 mg, 0.42 mmol); colorless solid of mp 235 °C (ethanol/*n*-hexane); ν_{max} (ATR)/cm^{-1}: 3003, 2968, 2932, 2608, 1622, 1590, 1544, 1486, 1461,

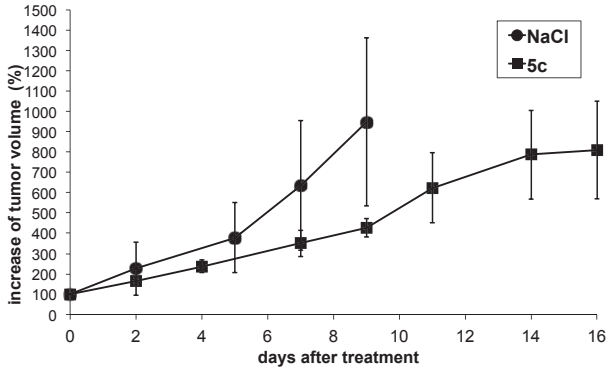

Fig. 8. Antitumor activity of **5c** in resistant A2780cis mouse xenograft tumors. Shown is the increase of mean tumor volumes of each group (n = 4) ± standard deviation normalized to day 0 (start of treatment). Mean tumor volumes at start of treatment were 218 mm^3 for the group treated i.p. with **5c** (40 mg/kg body weight on days 0, 3, 7, 10 and 14) and 204 mm^3 for the control group treated with saline. The tumors of the control group showed heterogeneous growth rates whereas tumors of mice treated with **5c** grew more slowly and more evenly leading to a narrower growth rate distribution at early stages. The treatment and monitoring of the control group was discontinued on day 9 when three mice had tumors exceeding 1500 mm^3 volume. On day 16, two tumors of the treatment group had exceeded 1500 mm^3.

1408, 1346, 1314, 1260, 1219, 1146, 1115, 1039, 995, 870, 854, 795, 749, 725, 677; ^{1}H NMR (300 MHz, DMSO-d_6): δ 1.37 (3 H, t, ^3J 7.2 Hz), 3.56 (3 H, s), 3.64 (3 H, s), 3.66 (3 H, s), 4.29 (2 H, q, ^3J 7.2 Hz), 7.20 (1 H, d, ^4J 2.0 Hz), 7.3–7.4 (2 H, m), 7.71 (1 H, s), 7.8–7.9 (2 H, m), 9.38 (1 H, s); ^{13}C NMR (75.5 MHz, DMSO-d_6): δ 15.4, 33.9, 40.9, 55.7, 59.9, 93.0, 102.9, 111.7, 112.1, 117.0, 120.5, 124.5, 125.2, 125.3, 126.7, 127.5, 128.1, 130.8, 135.1, 135.4, 148.5, 152.0; *m/z* (EI) 523 (33) [M^+], 521 (100) [M^+], 506 (42); Anal $C_{22}H_{21}ClIN_3O_2$ (free base; C, H, N).

4.1.8. 2,3-Dichloro-1-methyl-5-[1-methyl-4-(3-bromo-4,5-dimethoxyphenyl)-imidazol-5-yl]indole hydrochloride (**5h**)

Analogously to the synthesis of **5b**, compound **5h** (90 mg, 41%) was obtained from **3c** (96 mg, 0.42 mmol), 33% $MeNH_2$/ethanol (260 μL, 2.10 mmol), acetic acid (150 μL), and **4c** (172 mg, 0.42 mmol); colorless solid of mp 152–155 °C (ethanol/*n*-hexane); ν_{max} (ATR)/cm^{-1}: 3003, 2937, 2837, 2590, 1623, 1595, 1547, 1490, 1464, 1405, 1361, 1318, 1263, 1238, 1152, 1116, 1042, 996, 976, 878, 853, 808, 758, 730, 680; ^{1}H NMR (300 MHz, DMSO-d_6): δ 3.61 (3 H, s), 3.64 (3 H, s), 3.70 (3 H, s), 3.86 (3 H, m), 7.13 (1 H, d, ^4J 2.0 Hz), 7.28 (1 H, d, ^4J 2.0 Hz), 7.40 (1 H, dd, ^3J 8.6 Hz, ^4J 1.2 Hz), 7.73 (1 H, d, ^4J 1.2 Hz), 7.84 (1 H, d, ^3J 8.6 Hz), 9.37 (1 H, s); ^{13}C NMR (75.5 MHz, DMSO-d_6): δ 30.9, 33.9, 56.1, 60.2, 101.0, 111.5, 112.0, 116.8, 118.2, 119.9, 122.4, 123.8, 124.4, 124.6, 125.6, 127.8, 130.5, 134.9, 135.6, 145.9, 153.3; *m/z* (EI) 497 (51) [M^+], 495 (100) [M^+], 493 (66) [M^+], 488 (24), 486 (53), 484 (33); Anal $C_{21}H_{18}BrCl_2N_3O_2$ (free base; C, H, N).

4.1.9. 2,3-Dichloro-1-ethyl-5-[1-methyl-4-(3-bromo-4,5-dimethoxyphenyl)-imidazol-5-yl]indole hydrochloride (**5i**)

Analogously to the synthesis of **5b**, compound **5i** (94 mg, 43%) was obtained from **3d** (102 mg, 0.42 mmol), 33% $MeNH_2$/ethanol (260 μL, 2.10 mmol), acetic acid (150 μL), and **4c** (172 mg, 0.42 mmol); colorless solid of mp 226–230 °C (ethanol/*n*-hexane); ν_{max} (ATR)/cm^{-1}: 2980, 2562, 1623, 1609, 1593, 1546, 1509, 1490, 1468, 1452, 1404, 1345, 1319, 1280, 1238, 1218, 1150, 1114, 1042, 996, 852, 807, 758; ^{1}H NMR (300 MHz, DMSO-d_6): δ 1.29 (3 H, t, ^3J 7.1 Hz), 3.58 (3 H, s), 3.63 (3 H, s), 3.70 (3 H, s), 4.39 (2 H, q, ^3J 7.1 Hz), 7.1–7.2 (2 H, m), 7.39 (1 H, dd, ^3J 8.6 Hz, ^4J 1.3 Hz), 7.74 (1 H, d, ^4J 1.3 Hz), 7.88 (1 H, d, ^3J 8.6 Hz), 9.33 (1 H, s); ^{13}C NMR (75.5 MHz, DMSO-d_6): δ 15.3, 34.4, 40.9, 56.4, 60.7, 101.8, 111.8, 112.3, 117.3, 118.8, 120.5, 122.9, 123.9, 124.5, 125.2, 125.8, 128.5, 131.0, 134.3, 136.1, 146.3, 153.7; *m/z* (EI) 511 (44) [M^+], 509 (100) [M^+], 507 (60) [M^+], 496 (22), 494 (52), 492 (27); Anal $C_{22}H_{20}BrCl_2N_3O_2$ (free base; C, H, N).

4.2. Cell lines and culture conditions

The human carcinoma cell lines HT-29 (colon), HCT-116 (colon), MCF-7 (breast), and KB-V1 (cervix) were purchased from The German Collection of Microorganisms and Cell Cultures (DSMZ, Braunschweig). MCF-7 and KB-V1 cells were rendered multidrug-resistant, indicated as MCF-7/Topo and KB-V1/Vbl, by repeated application of topotecan or vinblastin, respectively. The HUVEC-derived endothelial hybrid cell line Ea.hy926 was obtained from The American Type Culture Collection (ATCC no. CRL-2922). The human melanoma cell line 518A2 was a gift from the Department of Radiotherapy and Radiobiology, University Hospital Vienna. It is not available from cell banks, yet easily identified by its large size and its flat, spread-out morphology. The cells were grown in DMEM or RPMI (HT-29) medium, supplemented with 10% fetal bovine serum (FBS), 1% Antibiotic-Antimycotic solution (both from Gibco) and 250 μg/mL gentamycin (SERVA). Primary chicken heart fibroblasts (CHF) were explanted from 10 day-old chicken embryos and separated from other cell types for several weeks [29]. The established cell line from a single cell cluster of fibroblasts was finally grown in DMEM (10% FBS, 1% Anti–Anti, 250 μg/mL gentamycin) and used before the 20th passage. Chicken cardiomyocytes (CCM) were separated by trypsination of single pulsating cell clusters [29–31], grown to confluence in DMEM (20% FBS, 1% Anti–Anti, 250 μg/mL gentamycin) and used before the 3rd passage. All cells were incubated at 37 °C, 5% CO_2, 95% humidified atmosphere. Only mycoplasma-free cell lines were used.

4.3. Growth inhibition assays (MTT assay)

Inhibition of cell proliferation by CA-4 or the new derivatives was determined by using a standard MTT assay as previously described [32]. Briefly, cells grown in 96-well cell culture plates (5000 cells/well; Ea.hy926 and CHF: 10,000 cells/well, CCM: 20,000 cells/well) were treated with dilution series of CA-4, the derivatives **5a-i** (100 μM–5 pM) or respective amounts of DMSO (solvent controls) for 72 h. Cells were then incubated with MTT at a final concentration of 0.5 mg/mL for 2 h. The formazan precipitate was dissolved in 10% SDS, 0.6% acetic acid in DMSO and the absorbance at wavelength 570 and 630 (background) nm was measured with a microplate reader (Tecan). The percentage of viable cells was calculated with respect to DMSO-treated controls set to 100%. Half-maximal inhibitory concentrations (IC_{50}) are represented as the mean of at least three experiments ± standard deviation (S.D.). The relative selectivity of the compounds was represented as the relation of the logarithmic mean of IC_{50} values against cancer cells (CA-4-resistant HT-29 were excluded from this calculation for CA-4) and the mean (log) of IC_{50} values in non-malignant fibroblasts.

4.4. Cell cycle analyses and immunostaining of mitotic cells

For cell cycle analyses, HT-29 cells grown in 6-well cell culture plates (200,000 cells/well) were incubated with DMSO (control) or 100 nM of the indoles **5a** or **5c** for 24 h. Due to their resistance to CA-4, a high concentration of 5 μM was used to get a typical effect on the cell cycle progression. Cells were then harvested by trypsination, resuspended in 4% formaldehyde (in PBS) and fixed at room temperature for 20 min. For permeabilization, cells were incubated

with 90% ice-cold methanol for 30 min on ice prior to immunostaining (37 °C, 1 h) with a primary phospho-histone H3 antibody as a marker for mitosis (anti-phospho-histone H3 (Ser10), rabbit polyclonal antibody, Millipore; 5 μg/mL in 1% BSA/PBS) and a secondary antibody-AlexaFluor-488 conjugate (goat anti-rabbit-IgG-AlexaFluor-488 conjugate, Invitrogen). Cells were washed by centrifugation and stained with propidium iodide staining solution (50 μg/mL propidium iodide, 0.1% sodium citrate, 50 μg/mL RNase A in PBS) for 30 min at 37 °C. The fluorescence intensity of 10,000 single cells at an emission wavelength of 620 nm (propidium iodide fluorescence) and 525 nm (AlexaFluor-488 fluorescence; excitation with a 488 nm laser source) was recorded with a Beckman Coulter Cytomics FC500 flow cytometer and analyzed for the distribution (%) of single, viable (sub-G1 events < 3.5%) cells to G1, S, G2 and M phase of the cell cycle by using the CXP software (Beckman Coulter).

4.5. Tubulin polymerization assay

Alpha- and beta-tubulin heterodimers were purified from porcine brain by the method of Castoldi and Popov [33]. To start the polymerization to microtubules, equal volumes of 10 mg/mL tubulin stock solutions in BRB80 (Brinkley's buffer, 80 mM PIPES-KOH, 1 mM $MgCl_2$, 1 mM EGTA) and 2 × polymerization buffer (20% glycerol, 3 mM GTP in BRB80) containing CA-4, **5a**, **5c** (10 μM pre-dilution in BRB80) or equal amounts of DMSO (control) were mixed in pre-warmed, black 96-well plates (μClear® black 96-well plates, UV-star, Greiner bio-one). The polymerization was monitored at 37 °C by measuring the increase in the optical density at 340 nm every 20 s with a microplate reader (Tecan). Obtained polymerization curves were then normalized with respect to the starting absorbance values and are represented as the mean of two independent measurements in duplicates (S.D. of each time point <5%).

4.6. Molecular docking into the tubulin colchicine-binding site

Coordinate files of the ligand structures were generated using the GlycoBioChem PRODRG2 Server (http://davapc1.bioch.dundee.ac.uk/prodrg/submit.html) [34]. Molecular docking calculations were carried out using the Autodock Vina software [35]. For this, Gasteiger partial charges [36] were calculated on ligand atoms using Autodock Tools. The X-ray structure of the crystallized tubulin-colchicine complex (PDB accession code: 1SA0 [37]) was downloaded from the Protein Data Bank (http://www.rcsb.org) and later used for docking. As for the ligand, polar hydrogen atoms were added to the protein and Gasteiger partial charges were calculated using Autodock Tools. Water molecules, heteroatoms and ligands were removed from the structure prior to docking calculations. Residues Lys-β254, Lys-β352, Asn-α101, Val-β318 and Ile-β378 were treated as flexible residues. Simulation boxes were centered on the originally crystallized ligand colchicine. A 18 × 22 × 20 Å simulation box was used in the docking calculations, using an exhaustiveness option of 20. It should be noted that the standard error of Autodock Vina is 2.85 kcal mol^{-1} [35], which means that binding affinities cannot be quantitatively predicted *in silico* using docking calculations. In addition, the estimated coordinate error of the tubulin template structure, which was solved to a moderate resolution of 3.58 Å, already amounts to ~0.5 Å. Figures were prepared by means of the program PYMOL [38].

4.7. Immunofluorescence microscopy of the microtubule cytoskeleton

518A2 cells grown on glass coverslips in 24-well plates (25,000 cells/well) were incubated with 100 nM **5a** or **5c** for 24 h. After fixation (4% formaldehyde in PBS, 20 min, rt), permeabilization and blocking (0.1% Triton X-100, 1% BSA in PBS) of the cells, a primary antibody for alpha-tubulin (anti-alpha-tubulin, mouse, monoclonal antibody, Invitrogen/Life Technologies) was added in 1% BSA/PBS at 37 °C for 1 h and microtubules were visualized with a secondary goat anti-mouse-IgG-AlexaFluor-488 conjugate (Invitrogen/Life Technologies). Coverslips were then mounted into Mowiol 4-88-based mounting medium containing 1 μg/mL DAPI (both from Carl Roth) for counterstaining the nuclei. Immunofluorescence images were taken by using an Axio Imager.A1 fluorescence microscope (400-fold magnification, ZEISS).

4.8. Tube formation assay with Ea.hy926 endothelial cells

Ea.hy926 endothelial hybrid cells (100,000 cells/well) were seeded into 24-well plates onto glass coverslips coated with 10 μL of Matrigel™ basement membrane matrix (BD Biosciences; gelation for 30 min in a humidified atmosphere at 37 °C). The cells were allowed to differentiate into blood vessel precursor-like networks through growth factor stimulation within the next 12 h. Then, CA-4 (100 nM) or the indoles **5a** or **5c** (250 nM) were added to the wells for a further 16 h and a vascular-disruptive effect on the established cell network was documented by microscopy (Axiovert 135, ZEISS; 100-fold magnification). The viability of treated cells was additionally assessed by 2 h incubation with 200 μL 0.5 mg/mL MTT and subsequent determination of the formazan precipitate (*cf.* MTT assay description) by absorbance measurements. Viability in treated wells was calculated with respect to DMSO controls and was determined to be >90% when pictures were taken.

4.9. Chorioallantoic membrane (CAM) assay with fertilized chicken eggs [39]

White leg hen eggs (SPF eggs, VALO Biomedia) were incubated until day 5 after fertilization at 37 °C and 50–60% humidity. A window of 2–3 cm diameter was cut into the pole end of the eggshell and rings of silicon foil (6 mm diameter) were placed on the developing vessels within the CAM. Eggs were then sealed with sterile tape and incubated for a further 24 h. Dilutions of DMSO (control), **5a** or **5c** (500 μM in PBS) were directly pipetted inside the silicon ring (20 μL = 10 nmol, 10 μL = 5 nmol) and alterations in the blood vessel organization were documented 0 h, 12 h and 24 h post application with a stereomicroscope (Traveller, 60-fold magnification). For assessing effects on *in vivo* tumor growth with the CAM assay model, pellets of 1 × 10^6 HT-29 cells in 10 μL 1:1-mixture of matrigel and serum-free RPMI (gelled at 37 °C for 30 min) were directly placed on the CAM and incubated for 48 h until an interaction between the tumor pellets and the surrounding blood vessels was observed. 100 μL of a 50 μM dilution in PBS (5 nmol) of indole **5c** were then pipetted on the CAM outside of a silicon ring around the tumor pellet, incubated for 24 h and the changes were documented with a stereomicroscope (Traveller, 10-fold magnification). For histological examination, the micro-xenografts were explanted, fixed in 4% formalin and embedded in paraffin. Hematoxylin/eosin (HE) staining of tissue slices was performed according to standard protocols. Images shown in this paper are representative for at least three independent experiments with the same outcome.

4.10. Animal studies

The investigations of this study were approved by the Laboratory Animal Care Committee of Sachsen-Anhalt, Germany. Xenograft tumors were generated in athymic nude mice (Harlan and

Winkelmann, Borchen, Germany) using the germ cell tumor cell line 1411HP and the ovarian carcinoma cell line A2780cis. 8 Million cells of either cell line were resuspended in PBS and injected subcutaneously into the flank of mice. Both cell lines form highly vascularized xenograft tumors in nude mice and are resistant to various anticancer drugs. Xenografts of 1411HP were previously used as an established animal model for the test of vascular-disrupting activity [18,21]. To test compound **5c** for tumor vascular disrupting activity *in vivo*, 100 mg/kg bodyweight of it were administered by intraperitoneal injection. The resulting tumor discoloration was documented after 24 h with a Canon IXUS 50. For histological examination, the tumors were explanted, fixed in 5% formalin, and embedded in paraffin. Hematoxylin/eosin (HE) staining of the tissue slices was performed according to standard protocols. HE images were analyzed by microscopy (Axio Lab, Zeiss).

The antitumor activity of **5c** was analysed in nude mice bearing xenograft tumors grown from resistant A2780cis cells. After establishment of tumors the mice were divided in two groups ($n = 4$) with similar mean tumor volumes at the start of treatment (treatment group: 218 mm^3; control group: 204 mm^3). The mice received i.p applications of 40 mg/kg body weight on days 0, 3, 7, 10 and 14. The control group received normal saline. The tumor volumes were calculated by caliper measurement using the formula $a^2 \times b \times 0.5$ with a being the short and b the long dimension.

Conflict of interest

The authors declare that there are no conflicts of interest.

Acknowledgment

We are indebted to Franziska Reipsch (Department of Internal Medicine IV, Halle) for her excellent technical assistance.

Appendix A. Supplementary data

Supplementary data related to this article can be found at http://dx.doi.org/10.1016/j.ejmech.2016.04.045.

References

[1] G.R. Pettit, S.B. Singh, E. Hamel, C.M. Lin, D.S. Alberts, D. Garcia-Kendall, Experientia 45 (1989) 209–211.
[2] C.J. Mooney, G. Nagaiah, P. Fu, J.K. Wasman, M.M. Cooney, P.S. Savvides, J.A. Bokar, A. Dowlati, D. Wang, S.S. Agarwala, S.M. Flick, P.H. Hartman, J.D. Ortiz, P.N. Lavertu, S.C. Remick, Thyroid 19 (2009) 233–240.
[3] G.C. Tron, T. Pirali, G. Sorba, F. Pagliai, S. Busacca, A.A. Genazzani, J. Med. Chem. 49 (2006) 3033–3044.
[4] J.W. Lipperts, Bioorg. Med. Chem. 15 (2007) 605–615.
[5] S.E. Holwell, P.A. Cooper, M.J. Thompson, G.R. Pettit, L.W. Lippert, S.W. Martin, M.C. Bibby, Anticancer Res. 22 (2002) 3933–3940.
[6] L.K. Folkes, M. Christlieb, E. Madej, M.R.L. Stratford, P. Wardman, Chem. Res. Toxicol. 20 (2007) 1885–1894.
[7] T. Brown, H. Holt, M. Lee, Heterocyclic Antitumor Antibiotics, Springer, Berlin, Heidelberg, 2006.
[8] L. Wang, K.W. Woods, Q. Li, K.J. Barr, R.W. McCroskey, S.M. Hannick, L. Gherke, R.B. Credo, Y.H. Hui, K. Marsh, R. Warner, J.Y. Lee, N. Zielinski-Mozng, D. Frost, S.H. Rosenberg, H.L. Sham, J. Med. Chem. 45 (2002) 1697–1711.
[9] N.R. Madadi, N.R. Penthala, K. Howk, A. Ketkar, R.L. Eoff, M.J. Borrelli, P.A. Crooks, Eur. J. Med. Chem. 103 (2015) 123–132.
[10] G.R. Pettit, M.D. Minardi, H.J. Rosenberg, E. Hamel, M.C. Bibby, S.W. Martin, M.K. Jung, R.K. Pettit, T.J. Cuthbertson, J.-C. Chapius, J. Nat. Prod. 68 (2005) 1450–1458.
[11] S. Ahn, C.B. Duke, C.M. Barrett, D.J. Hwang, C.-M. Li, D.D. Miller, J.T. Dalton, Mol. Cancer Ther. 9 (2010) 2859–2868.
[12] R. Romagnoli, P.G. Baraldi, T. Sarkar, M.D. Carrion, C.L. Cara, O. Cruz-Lopez, D. Preti, M.A. Tabrizi, M. Tolomeo, S. Grimaudo, A. Di Cristina, N. Zonta, J. Balzarini, A. Brancale, H.-P. Hsieh, E. Hamel, J. Med. Chem. 51 (2008) 1464–1468.
[13] D. Simoni, F.P. Invidiata, M. Eleopra, P. Marchetti, R. Rondanin, R. Baruchello, G. Grisolia, A. Tripathi, G.E. Kellogg, D. Durrant, R.M. Lee, Bioorg. Med. Chem. 17 (2009) 512–522.
[14] Q. Zhang, Y. Peng, X.I. Wang, S.M. Keenan, S. Arora, W.J. Welsh, J. Med. Chem. 50 (2007) 749–754.
[15] S. Arora, X.I. Wang, S.M. Keenan, C. Andaya, Q. Zhang, Y. Peng, W.J. Welsh, Cancer Res. 69 (2009) 1910–1915.
[16] (a) M.T. MacDonough, T.E. Strecker, E. Hamel, J.J. Hall, D.J. Chaplin, M.L. Trawick, K.G. Pinney, Bioorg. Med. Chem. 21 (2013) 6831–6843; (b) T.E. Strecker, S.O. Odutola, R. Lopez, M.S. Cooper, J.K. Tidmore, A.K. Charlton-Sevcik, L. Li, M.T. MacDonough, M.B. Hadimani, A. Ghatak, L. Liu, D.J. Chaplin, R.P. Mason, K.G. Pinney, M.L. Trawick, Cancer Lett. 369 (2015) 229–241.
[17] Z. Wen, J. Xu, Z. Wang, H. Qi, Q. Xu, Z. Bai, Q. Zhang, K. Bao, Y. Wu, W. Zhang, Eur. J. Med. Chem. 90 (2015) 184–194.
[18] R. Schobert, B. Biersack, A. Dietrich, K. Effenberger, S. Knauer, T. Mueller, J. Med. Chem. 53 (2010) 6595–6602.
[19] B. Biersack, Y. Muthukumar, R. Schobert, F. Sasse, Bioorg. Med. Chem. Lett. 21 (2011) 6270–6273.
[20] R. Schobert, K. Effenberger-Neidnicht, B. Biersack, Int. J. Clin. Pharmacol. Ther. 49 (2011) 71–72.
[21] K. Mahal, B. Biersack, H. Caysa, R. Schobert, T. Mueller, Invest. New Drugs 33 (2015) 541–554.
[22] R. Spagnuolo, S. Recalcati, L. Tacchini, G. Cairo, Br. J. Pharmacol. 163 (2011) 299–312.
[23] I. Mikaelian, A. Buness, M.-C. de Vera-Mudry, C. Kanwal, D. Coluccio, E. Rasmussen, H.W. Char, V. Carvajal, H. Hilton, J. Funk, J.C. Hoflack, M. Fielden, F. Herting, M. Dunn, L. Suter-Dick, Toxicol. Sci. 117 (2010) 144–151.
[24] C. Kanthou, O. Greco, A. Stratford, I. Cook, R. Knight, O. Benzakour, G. Tozer, Am. J. Pathol. 165 (2004) 1401–1411.
[25] T.L. Nguyen, C. McGrath, A.R. Hermone, J.C. Burnett, D.W. Zaharevitz, B.W. Day, P. Wipf, E. Hamel, R. Gussio, J. Med. Chem. 48 (2005) 6107–6116.
[26] C. Kanthou, G.M. Tozer, Expert Opin. Ther. Targets 11 (2007) 1443–1457.
[27] C. Kanthou, G.M. Tozer, Int. J. Exp. Pathol. 90 (2009) 284–294.
[28] M. Klingenberg, J. Becker, S. Eberth, D. Kube, J. Wilting, BMC Cancer 14 (2014) 339.
[29] T. Lindl, J. Bauer, Zell- und Gewebekultur: Einführung in die Grundlagen sowie ausgewählte Methoden und Anwendungen, G. Fischer, Stuttgart, 1994.
[30] J.W. Sanger, B. Mittal, J.M. Sanger, Cell Motil. 4 (1984) 405–416.
[31] A. Du, J.M. Sanger, K.K. Linask, J.W. Sanger, Dev. Biol. 257 (2003) 382–394.
[32] C. Spoerlein, K. Mahal, H. Schmidt, R. Schobert, J. Inorg. Biochem. 127 (2013) 107–115.
[33] M. Castoldi, A.V. Popov, Protein Expr. Purif. 32 (2003) 83–88.
[34] A.W. Schüttelkopf, D.M.F. van Aalten, Acta Crystallogr. D. Biol. Crystallogr. 60 (2004) 1355–1363.
[35] O. Trott, A.J. Olson, J. Comput. Chem. (2010) 455–461.
[36] J. Gasteiger, M. Marsili, Tetrahedron 36 (1980) 3219–3228.
[37] R.B. Ravelli, B. Gigant, P.A. Curmi, I. Jourdain, S. Lachkar, A. Sobel, M. Knossow, Nature 428 (2004) 198–202.
[38] W. DeLano, The PyMOL Molecular Graphics System, DeLano Sci. LLC, San Carlos CA, 2003.
[39] B. Nitzsche, C. Gloesenkamp, M. Schrader, M. Ocker, R. Preissner, M. Lein, A. Zakrzewicz, B. Hoffmann, M. Hoepfner, Br. J. Cancer 103 (2010) 18–28.